IDENTIFICATION	REVISION
FFDC04223-EN	3.0

AREVA NP
Fuel BU

AREVA

TOTAL NUMBER OF PAGES: 45

TRANSPORTATION IN FCC CONTAINER MECHANICAL ASPECTS RELATED TO A CHANGE IN THE FUEL ASSEMBLY MATERIALS

ADDITIONAL INFORMATION:

PROJECT	
HANDLING	Restricted AREVA
CATEGORY	STR - Study Report
STATUS	BPE

DISTRIBUTION TO	PURPOSE OF DISTRIBUTION

ROLES	NAMES	DATES	ORGANIZATIONS	SIGNATURES
AUTHOR REVIEWER APPROVER	[redacted]			

RELEASE DATA:

CHANGE CONTROL RECORDS:
This document, when revised, must be reviewed or approved by following regions:

France: Y
USA: N
Germany: N

Classification Export AL: 0E001 ECCN: N
Les marchandises portant la désignation "AL inégal N" sont soumises à la réglementation européenne ou allemande en matière de contrôle des exportations au sein ou hors de l'UE. Les marchandises portant la désignation "ECCN inégal N" sont soumises à la réglementation américaine. Les marchandises portant les désignations "AL:N" ou "ECCN:N" peuvent, selon la destination ou l'utilisation finales du produit, également être soumises à autorisation.

Export classification AL: 0E001 ECCN: N
Goods labeled with "AL not equal to N" are subject to European or German export authorization when being exported within or out of the EU. Goods labeled with "ECCN not equal to N" are subject to US reexport authorization. Even without a label, or with label "AL: N" or "ECCN: N", authorization may be required due to the final whereabouts and purpose for which the goods are to be used.

Exportkennzeichnung AL: 0E001 ECCN: N
Die mit "AL ungleich N" gekennzeichneten Güter unterliegen bei der Ausfuhr aus der EU bzw. innergemeinschaftlichen Verbringung der europäischen bzw. deutschen Ausfuhrgenehmigungspflicht. Die mit "ECCN ungleich N" gekennzeichneten Güter unterliegen der US-Reexportgenehmigungspflicht. Auch ohne Kennzeichen, bzw. bei Kennzeichen "AL: N" oder "ECCN: N", kann sich eine Genehmigungspflicht, unter anderem durch den Endverbleib und Verwendungszweck der Güter, ergeben.

NON-PROPRIETARY DOCUMENT

REVISIONS

REVISION	DATE	EXPLANATORY NOTES
3.0	See 1st page release date	Translation of modifications in the reference French version from version B to version 3.0 – See References, chapter 1, 4.2.3, 4.2.3.4, 4.2.3.4.2, 4.2.3.4.5, 4.2.3.5.1, 4.2.3.5.2, 4.2.3.5.3, Figure 11, Figure 18, and Figure 20.

TABLE OF CONTENTS

LIST OF APPENDICES

LIST OF FIGURES

REFERENCES

[1] TFX/DC/2087 (A) of 4/06/1998 "Conteneur prototype N°1. Rapport d'essais de chute ("Container prototype N°1. Drop test report")

[2] TFX/DC/2132 (B) of 17/05/1999 "Conteneur prototype N°2. Rapport d'essais de chute" ("Container prototype N°2. Drop test report ")

[3] Christian Lalanne : Vibration et chocs mécaniques – Tome 6 – Analyse pratique des mesures – Lavoisier 2004 (Vibration and mechanical shocks – Volume 6 – Practical analysis of measurements)

[4] Note FFTT/03/0014 of April 7 2003 " Further characterization of mock-ups after drop tests "

[5] DOS-12-00057684 FCC3 Chapitre 2.1 – Analyse structurelle (Chapter 2.1 Structural analysis)

[6] DOS-12-00057682 FCC4 Chapitre 2.1 – Analyse structurelle (Chapter 2.1 Structural analysis)

1. PURPOSE

The regulatory tests provided justification of the safety criteria for the transportation in FCC containers of fuel assemblies with structures and fuel rods made of zircaloy-4. The applicability of these results to other materials has to be demonstrated.

This design note sums up the actions and evaluations to justify the mechanical strength of the package in case of a change in cladding or structural materials with respect to the reference Zircaloy 4. In particular, it deals with the case of the M5 alloy at -40°C and [redacted] °C for a strain rate of [redacted] s^{-1}.

The proposed approach is to define a range of material mechanical properties which is acceptable with respect to the considered accident situations.

2. CONTAINER JUSTIFICATION IN ACCIDENT SITUATION: MECHANICAL ASPECTS

Regarding the mechanical aspects, the current file justifying the transportation of fuel assemblies in FCC containers relies upon two series of drop tests on packages containing AFA type fuel assembly mock-ups made of Zircaloy 4. These tests and mock-ups are described in refs [1] and [2].

For the record, the regulatory mechanical trials feature the following tests:

- Drop onto a bar from a height of 1 m,
- Drop from a height of 9 m for which the search for the worst-case situation leads to evaluation of the following cases:
  - Drop from 9 m, container in vertical position.
  - Drop "flat" from 9 m, with the container upside down and an inclination leading to maximum whipping effect.

Note that as developed today, the whole approach to package justification relies upon the fact, observed during the drop tests, that the integrity of the fuel rods is preserved at the end of the above mechanical trials.

3. DAMAGE TO THE CONTAINER

The nature of the cladding and structural materials has no significant effect on the distribution of the package masses or on its equivalent impact stiffness, which are primarily determined by the structure of the container. This means that the overall behavior of the package during impact is practically independent of the exact nature of the claddings and skeleton.

As a result, the available drop tests are a useable reference in respect of the energy absorbed by the container, the damage resulting from the latter and the inertia loading sustained by the assemblies.

As a consequence, the justification of the satisfactory container behavior established on the basis of the drop test results [1] and [2] is unaffected by a change in the fuel assembly cladding or structural materials.

4. DAMAGE TO THE FUEL ASSEMBLIES

The drop tests led to the plastic deformation of the skeleton (grids, guide thimbles, nozzles) and of the fuel rods in the assembly mock-ups. In each case, we shall examine the potential consequences of the observed damage and the impact, if any, of the assembly material properties on the latter.

4.1. SKELETON DEFORMATION

The drop onto a bar from a height of 1 m basically aims to test the resistance of the assembly to perforation. It does not constitute the design basis in respect of the inertia loads exerted on the assemblies.

The 9 m vertical drop mainly leads to the plastic deformation of the nozzle and guide thimble span located on the impact side under the inertia loading of the rods and has little effect on the overall geometry of the tube bundle. These skeleton deformations have no effect on the container safety.

The main phenomenon observed during the 9 m flat drop tests is the compaction of the tube bundle owing to the deformation of the grids under the effect of the fuel rod inertia. More precisely, the rod array tends towards a triangular compact stack through the plastic deformation of the grid straps.

It is therefore possible that the mechanical properties of the grid material will have an effect on the grid deformation amplitude, but the bundle geometry after the test will be overall and in all cases more compact than that of the initial array. From the point of view of the thermal test modeling and the criticality safety study hypotheses, rod bundle compacting is a favorable phenomenon. Insofar as neither the thermal test modeling nor the criticality study studies take into account this compacting, the deformation amplitude of the grids is not a parameter that will be considered in this study.

4.2. FUEL ROD DEFORMATIONS

The focus of the study will be on the loadings experienced by the rods; the relevant criterion is the preservation of integrity, a condition adequate for guaranteeing compliance with the safety requirements. For each of the regulatory drop cases, a review will be made of the damage observed during the tests, the potential risk arising from a change in the material mechanical properties and the available justification data.

4.2.1. DROP ON BAR

The deformations of the fuel assembly and in particular of the rod bundle close to the impacted zone are imposed by the deformation of the container and are less than those due to the flat drop from a height of 9 m.

4.2.2. VERTICAL DROP

In case of a vertical drop, the rods slip relatively to the grids and come in contact with the nozzle, which deforms plastically under the load.

Some rods pass through the nozzle plate others go round the outside of the nozzle. The result is bending deformation of these rods, distributed over one or two spans and limited in amplitude by the cavity dimensions.

The deformation of the rods is therefore not limited to their own strength, but by that of the structures which surround them. From this point of view, the vertical drop exerts less stress than the flat drop for which the compensation of the gaps is directed uniformly and may lead to larger deformation amplitudes.

4.2.3. FLAT DROP FROM A HEIGHT OF 9 M WITH WHIPPING EFFECT

The rods are subjected to bending deformation and load the grids under the transverse inertial loading related to deceleration during impact. The maximum available bending deflection, limited by the compact stacking of the rods, gets smaller with proximity to the impacting wall (see *figure 1*).

The identified risk is the concentration of the bending deformation of the claddings at their clamping location in the grids. The proposed demonstration is organized into the following steps:

1. Analysis of the dynamic loading conditions and equivalent static loading
2. Results of the post-test drop characterizations
3. Experimental analysis of the permissible deformations (rod bending)
4. Simulation of the rod bending tests
5. Deduction of the permissible elongation limits for the tested products

6. Simulation of the real-world container drop case at the rod bottom span
7. Extrapolation of this result to the other material properties
8. Elongations required for the various materials
9. Remark on the analysis uncertainties
10. Justification of the strength of the cladding for several materials
11. Definition of an acceptance criterion

4.2.3.1. ANALYSIS OF THE DYNAMIC LOADING CONDITIONS AND EQUIVALENT STATIC LOADING

The acceleration measured on the container cradle is presented in figure 2. At time 0.125 s, there occurs a hard shock between the cradle and the outer shell which generates an acceleration of about [redacted] g for [redacted] ms , in other words for a "frequency" of [redacted] Hz.

The shock response spectrum is in particular analyzed in [3]. It is worth noting that as long as the system frequency is less than the shock frequency, the equivalent static acceleration increases proportionally to frequency.

At the first span, the natural frequency of a rod under low-amplitude lateral loading is equal to [redacted] Hz. For larger amplitudes, the « apparent » frequency increases:

- Through the membrane tensile effect,
- Through the participation of the pellets in the rod stiffness,

and decreases:

- Under the effect of material yielding,
- Through the effect of elongation of the beam mid-fiber (slippage at the supports).

The results of the simulation calculations ([redacted]) show that the global trend is clearly towards decreases in the frequencies: on the one hand, the membrane stresses are very small on the end spans and on the other the participation of the pellets in the stiffness only plays an important role for small radii of curvature, therefore very locally on the rod whereas yielding plays a predominant role.

To sum up, the change from a Zircaloy-4 material to a material with different mechanical properties leads to modification of the apparent frequency, which results in variation of the equivalent static loading in the ratio of these natural frequencies. The deformation amplitudes are therefore as a first approximation inversely proportional to the square root of the apparent stiffnesses, which leads to a constant strain energy irrespective of the material. Digital simulation on a simple oscillator subjected to an acceleration step shows that this energy conservation is confirmed at better than [redacted] % in the [redacted] Hz frequency band.

Remark on the presence of a stop

A simplified mechanical model (linear beams + springs) of the rod was built to check that the presence of a stop of near-infinite stiffness does not lead to an increase of apparent frequency liable to raise the equivalent static loading. The result, presented in figure 3, shows that the presence of a stop does increase the apparent natural frequency but that the latter remains moderate and does not therefore challenge the conclusions of this section. This result is explained by the bending behavior of the rod, which is quite different from a simple mass / spring system.

Moreover, the presence of a stop leads to a sharp reduction in the bending moment which comfortably compensates for the increase in equivalent static loading arising from the rise in apparent natural frequency.

4.2.3.2. RESULT OF THE POST-TEST DROP CHARACTERIZATIONS

A non-destructive examination of the mock-ups which underwent the drop tests was carried out with the main aim of determining the damage to the fuel assembly [4].

The most-deformed rods are those in the layer opposite the impact, at the bottom span of the [redacted] ft mock-up (as a reminder, the flat test was carried out for the container upside down). This is consistent with the fact that:

- This layer is the one which exhibits the most freedom of transverse displacement,
- The [redacted] assemblies have a bottom span height of [redacted] mm, which is much greater than for the [redacted] assemblies (about [redacted] mm) and therefore are substantially more flexible at this span location,
- The boundary conditions on the end grid side enable rod slippage along its axis, which helps to limit the membrane effect, therefore the increase in stiffness,
- The clamping stiffness of the mixing grids is much greater than for the end grids, due to the rod bending symmetry effect on each side of the grid,
- The whip effect imposed during the test increases the accelerations in the lower part of the assembly.

Figure 4 presents the values measured at various points for the most-deformed rods. In parallel, the grids exhibit residual crushing of about [redacted] to [redacted] mm.

The table below sums up the characteristic values used for the remainder of the study.

PROPRIETARY TABLE

	Residual lateral bending deformations with respect to the supports (mm)		
	¼ span height	Mid-span	¾ span height
Rod #13 constituting the adopted upper-bound case	[redacted]	[redacted]	[redacted]

4.2.3.3. EXPERIMENTAL ANALYSIS OF THE PERMISSIBLE BENDING DEFORMATIONS

Bending tests were carried out on rods with M5 and Zircaloy-4 claddings at 20°C and in quasi-static.

Test 1

A first test, of the "three point bending" type, led to deformation of a rod with M5 cladding equipped with tungsten carbide pellets (length [redacted]) pressurized to [redacted] bars. The distance between supports was [redacted] mm and the load was applied through an AFA 2G grid unit consisting of a set of 3 X 3 cells. The pressure was continuously monitored, which enables any loss of integrity to be detected.

The test was continued up to a center deflection of [redacted] mm without loss of integrity. The examination of the rods did not show any localized marks at the interface between pellets or at the contact with the grid cell.

At this stage, the test was interrupted for reasons related to the geometrical compatibility.

Tests 2

To reinforce the previous approach, two additional 3 point bending tests were carried out with a distance between supports reduced to [redacted] mm in order to achieve minimum radius of curvature and to approximate to the real-world case (see figure 5). The supports consist in ball bearings (no friction) with a diameter of [redacted] mm.

One rod had a cladding made of zircaloy-4 and another had a cladding made of M5. The mechanical properties of the cladding materials measured on the product were recorded. The tested claddings are taken from the manufactured batch, without any prior geometrical specification. The overall length of the cladding is [redacted] mm.

The pellets are made of tungsten carbide (WC) with a diameter of [redacted] mm and a length of [redacted] mm. They have no chamfer or dishing contrarily to the UO2 pellets. The toughness of the WC pellets ([redacted]) is noticeably higher than the UO2 pellets one, what is increasing the damaging of the cladding and so the severity of the test. They are hold by an AFA3G rod spring.

As for the previous test, the pressure was continuously monitored to detect any loss of integrity.

The figure 6 shows the experimental installation and the global shape of the specimen.

For zircaloy-4, the deflection which led to the loss of integrity is equal to [redacted] mm. The residual radius of curvature was [redacted] mm, which corresponds to an "apparent elongation at load" of [redacted] %.

For M5, the test was carried out up to a deflection of [redacted] mm without loss of integrity. The rod was then tested in the crosswise direction to bring the ends closer and identify the ultimate tensile strength.

When the rod ends were at [redacted] mm from each other, the loss of integrity was observed at the same time as the cladding failure. The average radii of curvature measured at the end of each of the phases were used to assess the apparent elongation values reached:

- After phase 1, the residual radius of curvature was [redacted] mm, or an "apparent elongation at load" of [redacted] %,
- At the time of rupture, the radius of curvature measured at load was [redacted] mm, or an "apparent elongation at load" of [redacted] %.

The actual elongation in the material is of course far higher than the above values because in particular of the mid-fiber shifts and the strain concentrations at the inter-pellet joints, and even a local necking.

Figure 7 illustrates the maximum deflection reached on M5 material (first compression phase) and figure 8 shows the force/deflection curves obtained for both materials and figure 9 the shape of the rods after the rupture.

Note that the shape of the curves not only reflects the elastic/plastic behavior of the material, but also the geometrical non-linearity. Indeed, as the distance between supports is constant, the beam mid-fiber elongates very significantly for the deflections reached. In parallel, the diameter of the rolls forming the beam support ([redacted] mm) influences the rod boundary conditions.

4.2.3.4. SIMULATION OF THE BENDING TESTS TO DEDUCE THE LIMIT APPARENT ELONGATIONS

A modeling attempt by means of finite element calculations ended with a failure as the relationships to be imposed between the cladding and the pellets are complex and evolve with the applied deflection. The finite element calculations without inclusion of the pellets lead to unrealistic results regarding the maximum plastic strains on the cladding (creation of plastic knobs which do not exist in reality because of the reinforcement supplied by the pellets).

Determination of the limit apparent elongations in the cladding materials leads to the following steps:

- Determination of the strain hardening curves for the tested materials
- Determination, for a given material and section, of the moment / curvature relationship (see appendix 1)
- Calculation of large-displacement beam bending by integrating into each element the previously determined moment / curvature relationship
- Empirical increase of the moment / curvature ratio by iterating the previous bending calculation to obtain the experimental results (force / deflection curves and elongations). It should be noted that this increase is used in the temperature range of -40°C to [redacted] °C, for quasi-static deformation of materials or for a rate of [redacted] s^{-1}.

- Deduction of the required apparent elongations of the cladding and comparison with the specified elongations.

4.2.3.4.1. DEFINITIONS

Regarding elongation, 3 different quantities are defined:

- The actual rupture elongation of the material under tensile load, corresponding to the maximum elongation measured on a tensile test specimen at the necking,
- The total elongation or rupture elongation determined during a tensile test at the terminals of the extensometer. For the cladding tube, the elongation is measured over a length of [redacted] mm,
- The apparent rupture elongation for a bending test measured from the minimum radius of curvature.

4.2.3.4.2. MECHANICAL PROPERTIES AND STRAIN HARDENING CURVES OF THE MATERIALS

The cladding characteristics used for the bending tests are as follows, at 20°C in quasi-static traction:

Cladding	Zr-4	M5
Sy 0.2 % (MPa)	[redacted]	[redacted]
Su (MPa)	[redacted]	[redacted]
A % (50 mm)	[redacted]	[redacted]

Material batch characteristics at 20°C in quasi-static traction

The relevant minimal characteristics for various cladding materials at 20°C in quasi-static loads are as follows:

Cladding	Zr-4 (min spec)	Duplex (min spec)	PCA-2b (min spec)	M5 (min spec)	Zr1Nb (min spec)
Sy 0.2 % (MPa)	[redacted]	[redacted]	[redacted]	[redacted]	[redacted]
Su (MPa)	[redacted]	[redacted]	[redacted]	[redacted]	[redacted]
A_t %(50 mm)	[redacted]	[redacted]	[redacted]	[redacted]	[redacted]

Minimum characteristics of the materials at 20°C in quasi-static traction coming from the technical specification

M5 alloy is also considered at temperatures of -40°C and [redacted] °C with a tensile strain rate of [redacted] (see §4.2.3.5.1). Tensile tests on specimens were done with these conditions. The average characteristics measured are as follows:

Cladding	M5, -40°C / [redacted]	M5, [redacted] °C / [redacted]
Sy 0.2 % (MPa)	[redacted]	[redacted]
Su (MPa)	[redacted]	[redacted]
A_t %(50mm)	[redacted]	[redacted]

Average characteristics of M5 alloy measured on specimens at -40°C and [redacted] °C in dynamical traction at [redacted]

During the same test campaign specimens were tested at 20°C in quasi-static traction. The average characteristics are given in the table below. These measures are close to those achieved since 2009 under the same conditions.

PROPRIETARY TABLE

Cladding	M5, +20°C, quasi-static
Sy 0.2 % (MPa)	[redacted]
Su (MPa)	[redacted]
A % (50 mm)	[redacted]

Average characteristics of M5 alloy measured on specimens at +20°C in quasi-static traction

The ratios between these measures and the minimum M5 specifications at 20°C in quasi-static traction are used to calculate minimum values for M5 cladding at -40°C and [redacted] °c in dynamical traction at [redacted] by extrapolation.

	Sy0.2% (MPa)	**Su(Mpa)**	**A%**
Test (average)	[redacted]	[redacted]	[redacted]
Mini spec			
Ratio	[redacted]	[redacted]	[redacted] ←

Calculation of the extrapolation ratios at minimal characteristics from measures and minimum specifications à 20°C in quasi-static traction

The minimum properties of M5 at -40°C and [redacted] °C under dynamical load at [redacted] are then calculated by means of these 3 ratios.

	Sy0.2% (MPa)	**Su(Mpa)**	**A%**
Test (average)	[redacted]	[redacted]	[redacted]
Mini spec(1)			
Ratio	[redacted]	[redacted]	[redacted] ←

Calculation of the minimal characteristics of M5 alloy at -40°C in traction at [redacted]

(1)Extrapolated equivalent of the minimum specification

	Sy0.2% (MPa)	**Su(Mpa)**	**A%**
Test (average)	[redacted]	[redacted]	[redacted]
Mini spec(1)			
Ratio	[redacted]	[redacted]	[redacted] ←

Calculation of the minimal characteristics of M5 alloy at [redacted] *°C in traction at* [redacted]

(1)Extrapolated equivalent of the minimum specification

PROPRIETARY TABLE

Cladding	M5, -40°C / [redacted] (mini spec)	M5, [redacted] °C / [redacted] (mini spec)
Sy 0.2 % (MPa)	[redacted]	[redacted]
Su (MPa)	[redacted]	[redacted]
A % (50 mm)	[redacted]	[redacted]

Minimal characteristics of M5 alloy at -40°C and [redacted] *°C in traction at* [redacted]

For all these materials, the strain hardening curves are deduced by assuming a law of the form:

$$\sigma = \sigma_0 + k \cdot \varepsilon_p^n ,$$

where n = [redacted] for Zircaloy-4, Duplex and PCA-2b and n = [redacted] for M5 and Zr1 Nb.

The considered strain hardening curves of the materials defined from the triplet (Sy, Su, At) are given in figures 10 and 11.

4.2.3.4.3. MOMENT / CURVATURE RELATIONSHIP

The method used to determine this bending moment / curvature relationship in a cladding section is explained in appendix 1.

4.2.3.4.4. CALCULATION SIMULATING THE BENDING TEST

The simulation calculation is carried out by means of 2 different methods, based on the same calculation principle and data:

- Use of the CASAC software (see appendix 2)
- Use of an EXCEL spreadsheet (see appendix 3)

The consistency of the results shown in figure 12 provides validation of the EXCEL approach, which will be the only one discussed hereafter (the CASAC calculation is limited to a deflection of about [redacted] mm and takes much longer in computing time).

The results obtained by strictly applying this method (cladding calculation only) are shown in figure 13 which compares with the test results. As expected, it can be seen that the calculated values are significantly lower than the measured values.

4.2.3.4.5. EMPIRICAL UPPER-BOUNDING OF THE MOMENT = F(CURVATURE) CURVE

As confirmed by the above calculation, the use of the moment / curvature relationships corresponding to the cladding only does not enable the test results to be obtained, as the contribution of the pellets plays an essential role in the overall behavior.

Moreover, the influence of the pellets is closely linked to the cladding material properties ([redacted]). As a result, for a given curvature value, a bending moment multiplier is needed.

On a fully decoupled basis, the next step is therefore to determine the moment multipliers needed to achieve the same test results for each of the 2 tested materials.

Figure 14 shows the calculation / test fit obtained with these multipliers. The maximum deflections achieved by calculation are about [redacted] mm. The bending moment achieved (therefore the apparent elongation) is then equal to its maximum value for Zircaloy-4 and quite similar for M5. The default reaching of the bending moment for M5 is a conservatism of the analysis.

Figure 15 represents the multipliers applied to carry out this fit. It can be clearly seen that the curvature / multiplier relationship follows a law which is non-trivial but near-similar for both materials and can be faithfully represented by a degree 2 polynomial.

This observation will enable us to extrapolate this calculation methodology and these multiplicative coefficients to the other materials. In addition, the identified coefficients are assumed to be independent of the temperature and strain rate.

4.2.3.4.6. ANALYSIS OF THE RESULTS IN TERMS OF ELONGATION

The calculation does not enable determination of the actual elongation of the material, but only the apparent elongations, determined from the minimum radii of curvature reached.

Determination of the actual elongation would call for a finite element calculation taking into account the pellet / rod contacts, which could not be done. Moreover, the specified elongation corresponds to a

total elongation over [redacted] mm. It is not directly comparable with the maximum actual elongation at the material final rupture location.

As a result, we shall stick to the notions of apparent elongation (related to the radii of curvature) and total elongation (measured during the standard tests).

The values obtained for a deflection of [redacted] mm are tabulated below:

Apparent elongation (%)	Zr4	M5
Test	[redacted]	[redacted]
Calculation (peak value)	[redacted]	[redacted]
Calculation (value integrated over 20 mm)	[redacted]	[redacted]

It can be seen that these measured apparent elongation values are slightly lower than the calculated peak values. This is naturally explained by the fact that the experimental elongation is determined from the radius of curvature, which integrates a given rod length whereas the calculated elongation corresponds to a highly localized value. The above table also shows the calculated elongations integrated over a length of [redacted] mm. These values are then much more consistent with the test values.

In these conditions, the measured and calculated elongations are similar, which helps to validate the analysis. Further, given the consistency of the results, this apparent elongation parameter is deemed relevant for comparing the various materials.

Bear in mind also that for M5, the cladding bending does not correspond to the product ultimate tensile strain but only to [redacted] % of the latter (see § 4.2.3.3).

4.2.3.4.7. LIMIT APPARENT ELONGATIONS; COMPARISON WITH THE RUPTURE ELONGATIONS

For zircaloy-4, the limit apparent elongation values correspond to the breaking point. The simulation results in § 4.2.3.4.6 directly supply an apparent elongation of [redacted] %.

For M5, the limit experimental value is [redacted] %. This value is increased of the ratio ([redacted]) in order to approach the pike value determined analytically. We therefore deduce that the product ultimate tensile strength is [redacted] %.

The table below compares the limit apparent elongations and the rupture elongations measured on the product.

Material	Apparent elongation (%)	Total elongation (%)	ratio
Zircaloy-4	[redacted]	[redacted]	[redacted]
M5	[redacted]	[redacted]	[redacted]

The main point is that there exists a ratio of about 2 between the rupture and apparent elongations. Hereafter, we shall adopt a ratio of [redacted] for Zircaloy-4, Duplex and PCA-2b and [redacted] for M5 and Zr1Nb. Note however that for M5, the apparent elongation is best-estimated by default (calculation deflection limited to [redacted] mm for a maximum in-test deflection of [redacted] mm) and that consequently the value of [redacted] is probably an upper-bound.

4.2.3.5. SIMULATION OF THE ACTUAL DROP CASE

4.2.3.5.1. CALCULATION WITH THE REFERENCE MATERIAL (ZIRCALOY-4)

The simulation calculation is detailed in appendix 4.

The objective of this calculation is to obtain the force-deflection curves of a Zircaloy-4 rod at the bottom span of the 900 MWe assembly. The equivalent static load is then best-fitted on the basis of the permanent deformation shape measurements at the mid-span, [redacted].

The results are shown in figure 16. The adopted equivalent static loading is [redacted] N. This force corresponds to the integral of the static equivalent load distributed on the rod. The permanent deformation shapes determined for this load value are as follows:

Residual deformation shape	¼ span	Mid-span	¾ span
Calculated value (mm)	[redacted]	[redacted]	[redacted]
Measured value (mm)	[redacted]	[redacted]	[redacted]

Note that the residual deformation shape is determined by means of the elastic stiffness calculated during load-up (return to zero is not calculated). However, it was checked that the elastic stiffness is near-similar up to a deflection greater than [redacted] mm at the center, which justifies the use of this method.

The maximum elongation (peak value) determined by the calculation is [redacted] %.

The strain energy is [redacted] J.

Otherwise, in the context of the licensing of the transportation in FCC containers of fuel assemblies with M5 cladding, it has been determined that the strain rate of the cladding during the drop test is [redacted]. The analysis leading to this estimate is presented in the safety report (see [5] and [6]). Furthermore it is necessary to consider transportation conditions at temperatures of -40°C and [redacted] °C.

4.2.3.5.2. CALCULATION FOR THE OTHER MATERIALS

The simulation results for the other materials at 20°C and the quasi-static deformation are shown in figure 17. The calculation results for M5 at -40°C and [redacted] °C under dynamical strain at [redacted] are shown in figure 18. The maximum deflection is determined so that the strain energy is in all cases identical to that calculated for Zircaloy-4.

The main results are tabulated below:

Material (*mini spec*)	**Zr-4**	**Duplex**	**PCA-2b**	**Zr1Nb**	
Temperature	[redacted]				
Strain rate	[redacted]				
Force	[redacted]	[redacted]	[redacted]	[redacted]	(N)
Deflection	[redacted]	[redacted]	[redacted]	[redacted]	(mm)
Strain energy	[redacted]				
Total apparent elongation	[redacted]	[redacted]	[redacted]	[redacted]	
Total elongation	[redacted]	[redacted]	[redacted]	[redacted]	
Plastic elongation	[redacted]	[redacted]	[redacted]	[redacted]	
Min Specification elongation	[redacted]	[redacted]	[redacted]	[redacted]	
Margin	[redacted]	[redacted]	[redacted]	[redacted]	

Material (*mini spec*)	M5			
Temperature	[redacted]	[redacted]	[redacted]	
Strain rate	[redacted]	[redacted]		
Force	[redacted]	[redacted]	[redacted]	(N)
Deflection	[redacted]	[redacted]	[redacted]	(mm)
Strain energy	[redacted]			
Total apparent elongation	[redacted]	[redacted]	[redacted]	
Total elongation	[redacted]	[redacted]	[redacted]	
Plastic elongation	[redacted]	[redacted]	[redacted]	
Min Specification elongation	[redacted]	[redacted]	[redacted]	
Margin	[redacted]	[redacted]	[redacted]	

The methodology implemented to perform these calculations, taking into account conservatisms, results in a positive margin between the calculated total elongation and the specified minimum elongation at material rupture.

4.2.3.5.3. CALCULATIONS FOR THE 1300 MWE ASSEMBLY CONFIGURATION

Given the energy-based approach in § 4.2.3.1, it seems less obvious that the 900 MWe configuration bounds the 1300 MWe one.

We shall therefore carry out the calculation of the 1300 MWe bottom span with the same principle and with the same tool as those used for the 900 MWe configuration.

The only difference is in the span length which changes from [redacted] mm to [redacted] mm. The length protruding below the bottom grid is kept at [redacted] mm.

The obtained force / deflection curves are shown in figure 19 for materials at 20°C in quasi-static strain. The calculation results obtained for M5 at -40°C and [redacted] °C with a strain rate of [redacted] are shown in figure 20.

This calculation is used for a strain energy reduced in the ratio of the beam lengths (the energy per mass unit is retained). The strain energy for the 1300 MWe assembly bottom span becomes: [redacted]

The results for the various materials are tabulated below:

Material (*mini spec*)	Zr-4	Duplex	PCA-2b	Zr1Nb	
Temperature	[redacted]				
Strain rate	[redacted]				
Force	[redacted]	[redacted]	[redacted]	[redacted]	(N)
Deflection	[redacted]	[redacted]	[redacted]	[redacted]	(mm)
Strain energy	[redacted]				
Total apparent elongation	[redacted]	[redacted]	[redacted]	[redacted]	
Total elongation	[redacted]	[redacted]	[redacted]	[redacted]	
Plastic elongation	[redacted]	[redacted]	[redacted]	[redacted]	
Min Specification elongation	[redacted]	[redacted]	[redacted]	[redacted]	
Margin	[redacted]	[redacted]	[redacted]	[redacted]	

Material (*mini spec*)	M5			
Temperature	[redacted]	[redacted]	[redacted]	
Strain rate	[redacted]	[redacted]		
Force	[redacted]	[redacted]	[redacted]	(N)
Deflection	[redacted]	[redacted]	[redacted]	(mm)
Strain energy		[redacted]		
Total apparent elongation	[redacted]	[redacted]	[redacted]	
Total elongation	[redacted]	[redacted]	[redacted]	
Plastic elongation	[redacted]	[redacted]	[redacted]	
Min Specification elongation	[redacted]	[redacted]	[redacted]	
Margin	[redacted]	[redacted]	[redacted]	

Comparison of this table with the one presented in § 4.2.3.5.2 shows that, although the forces and deflections are significantly different, the plastic elongation is very little impacted by the span length.

In the following, we shall retain the bounding elongations of the two studies.

4.2.3.6. REMARK ON THE ANALYSIS UNCERTAINTIES

The proposed approach presents simplifying hypotheses, some of which may appear debatable. However, throughout this analysis, the focus was always on remaining conservative.

For example:

- In the energy equivalence presented in § 4.2.3.1, it is assumed that the rod dampings are equivalent. However, the latter increase with deflection, partly because of pellet / cladding interaction and partly because of the environment of the other rods, which will exhibit a higher strength at elevated deflection. As an illustration, the change from [redacted] % to [redacted] % damping leads to an increase of about [redacted] % in the absorbed energy.
- The relationship between actual and apparent elongation is particularly conservative.
- The criterion is established by assuming a reduction in elongation, without accordingly reducing the ultimate tensile strength. As an illustration, for M5_min, the stress corresponding to [redacted] % elongation is only [redacted] MPa. Therefore, strictly speaking, the criterion could be expressed by the triplet ([redacted] MPa, [redacted] MPa, [redacted] %).

4.2.3.7. DEFINITION OF AN ACCEPTANCE CRITERION

A material having mechanical properties ($Sy_{0,2\ \%}$, Su) greater than a reference material will deform less than the latter under a given loading. As a reminder, the equivalent static loading will be in the ratio of the square roots of the stiffnesses, so the deflection will be inversely proportional to the ratio of the square roots of the stiffnesses.

As a result, the calculation results presented in the following paragraph will be translated into the double criterion, based on the definition, versus the material mechanical properties $Sy_{0,2\%}$ and Su, of a lower limit of the rupture elongation.

5. ACCEPTABLE MATERIAL PROPERTIES

5.1. STRUCTURAL MATERIAL

No specific criterion is adopted with respect to the structural materials.

In particular, the assumption is made that a change in the design or material of the grids would not significantly affect the conclusions presented below regarding the risk of clad failure.

5.2. CLADDING MATERIAL

Any material is acceptable if the criteria corresponding to one of the columns below are met:

		or	or	or	or	or
	$Sy_{0,2\%}$ (MPa) ≥	[redacted]	[redacted]	[redacted]	[redacted]	[redacted]
and	Su (MPa) ≥	[redacted]	[redacted]	[redacted]	[redacted]	[redacted]
and	At (% over 50 mm) ≥	[redacted]	[redacted]	[redacted]	[redacted]	[redacted]

If these criteria are not met, a dedicated study could be undertaken to check the acceptability of the material.

Figure 1
Compacting of the rod bundle

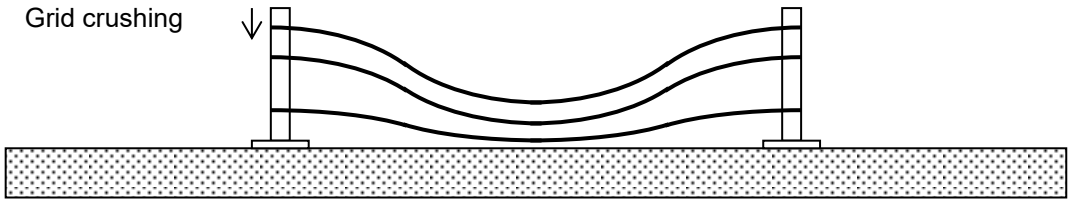

Figure 2
Acceleration measured on the leg side cradle

PROPRIETARY PICTURE

Figure 3
CASAC Calculation of a beam [redacted] mm long clamped at both ends

PROPRIETARY PICTURE

Figure 4
Characterization of the 12ft mock-up after drop test

PROPRIETARY PICTURE

Figure 5
Comparison compression test / actual test

PROPRIETARY PICTURE

PROPRIETARY PICTURE

Figure 6
Rod bending experimental device (2nd test)

PROPRIETARY PICTURE

PROPRIETARY PICTURE

Figure 7
Second 3-point bending test on M5 rods

[redacted]

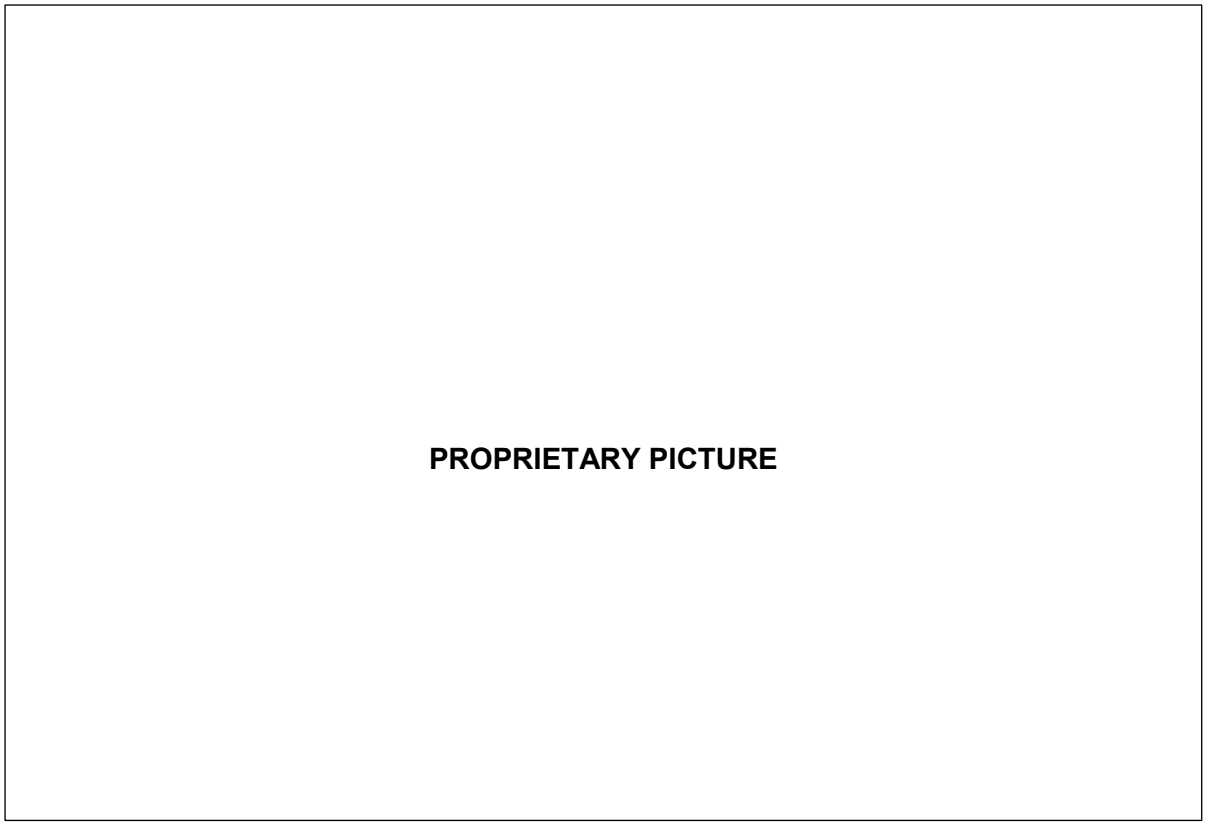

Figure 8
Rod bending test simply supported at both ends

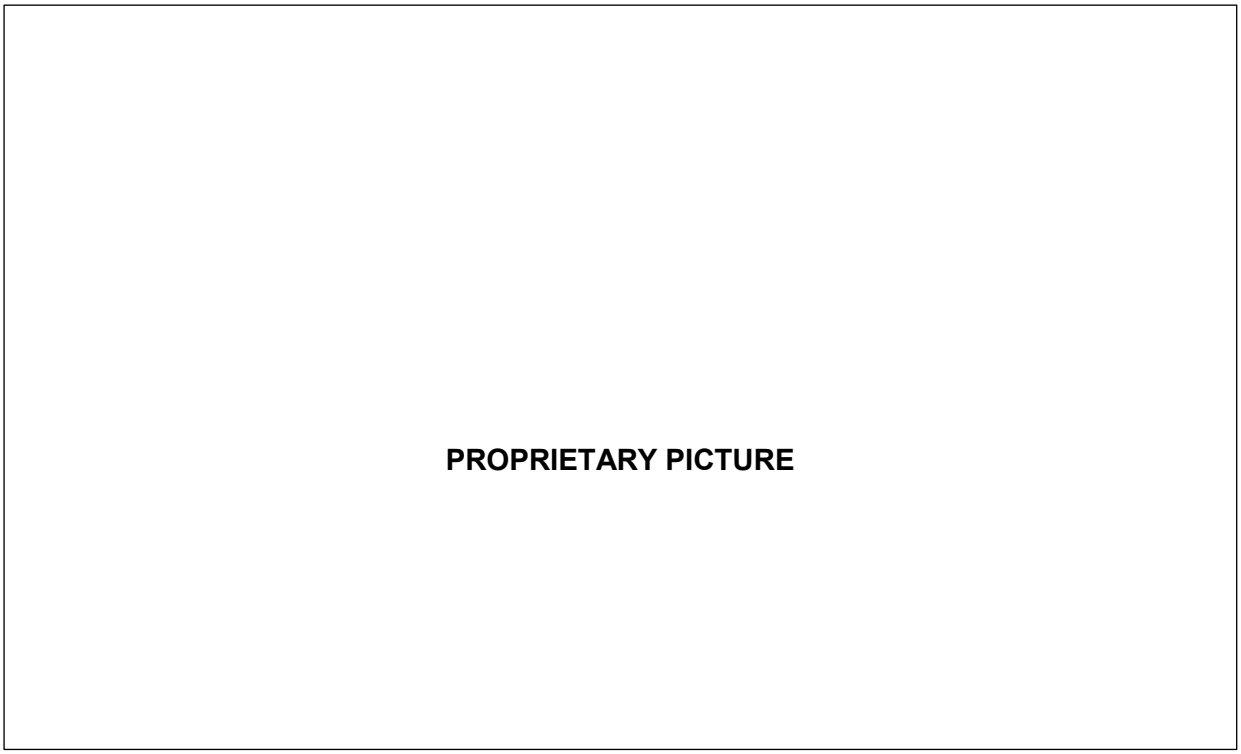

Figure 9
Shape of the rods after rupture

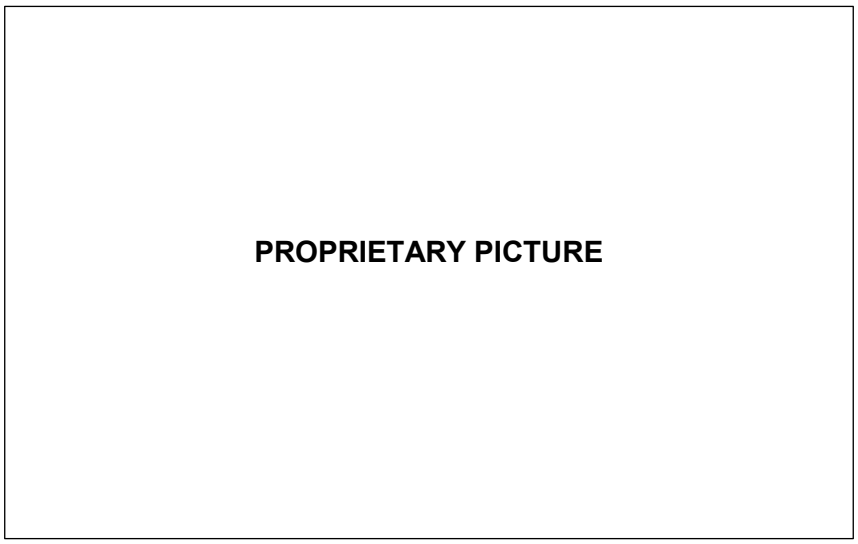

Zircaloy-4

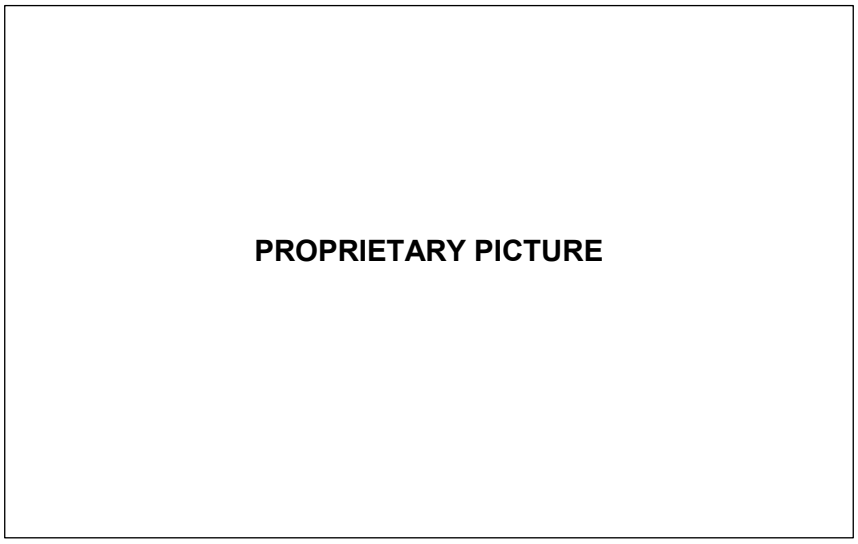

M5

Figure 10
Material strain hardening curves

PROPRIETARY PICTURE

Figure 11
Strain hardening curves for M5
at -40°C and [redacted] °C for
[redacted]

spec min *= minimum specification at 20°C in quasi-static strain*
[redacted]= extrapolated equivalent minimum specification in dynamical traction (see § 4.2.3.4.2)

PROPRIETARY PICTURE

Figure 12
Comparison CASAC / EXCEL calculations

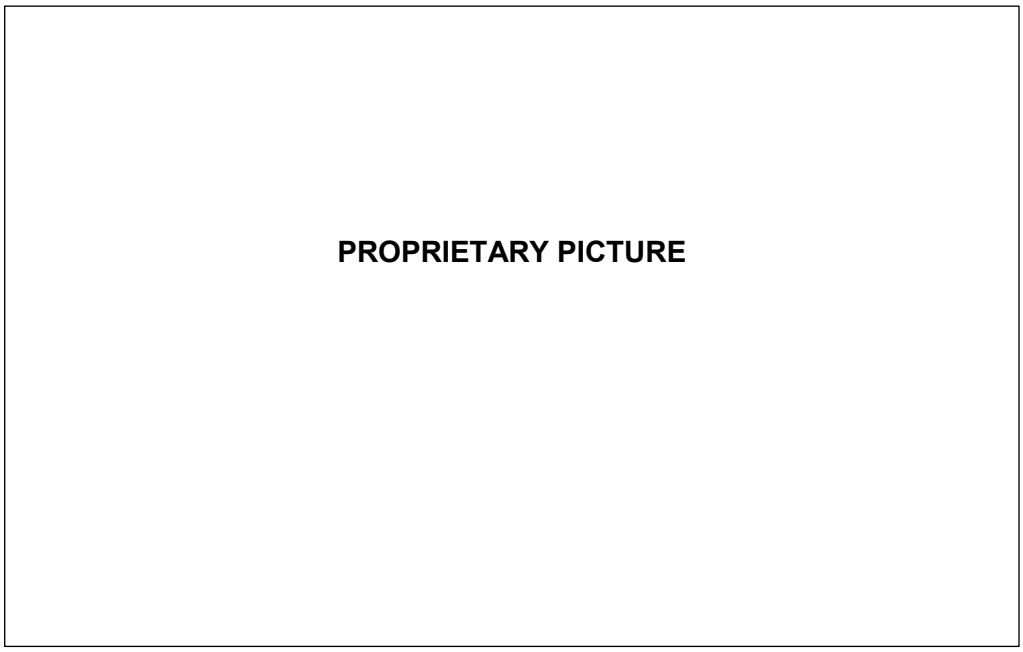

Figure 13
Force / deflection curves for the cladding alone at 20°C in quasi-static deformation

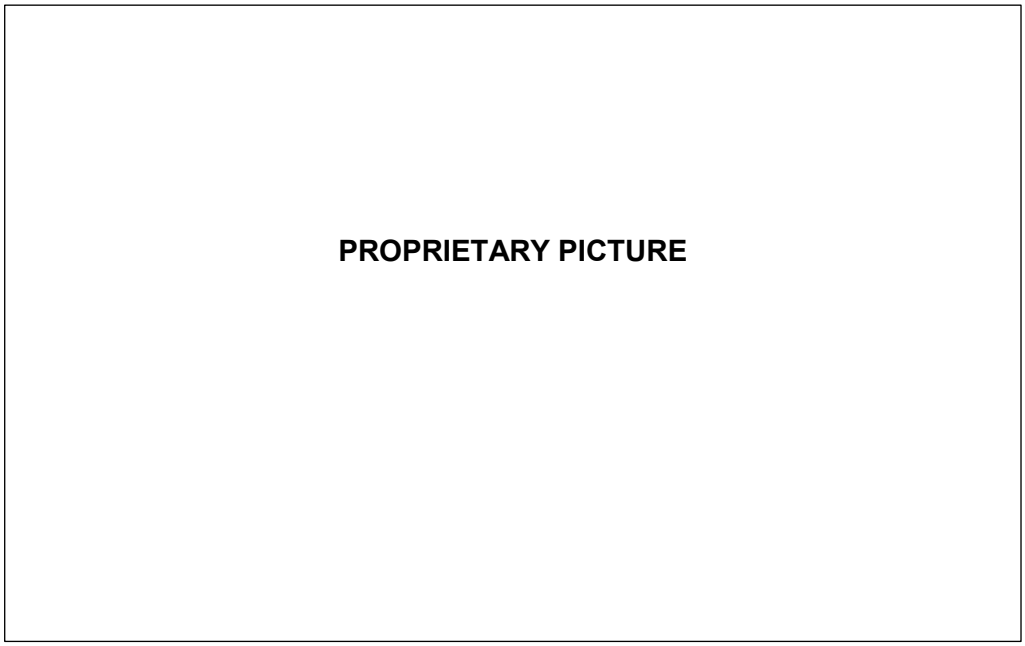

Figure 14
Calculation / test best fit at 20°C in quasi-static deformation

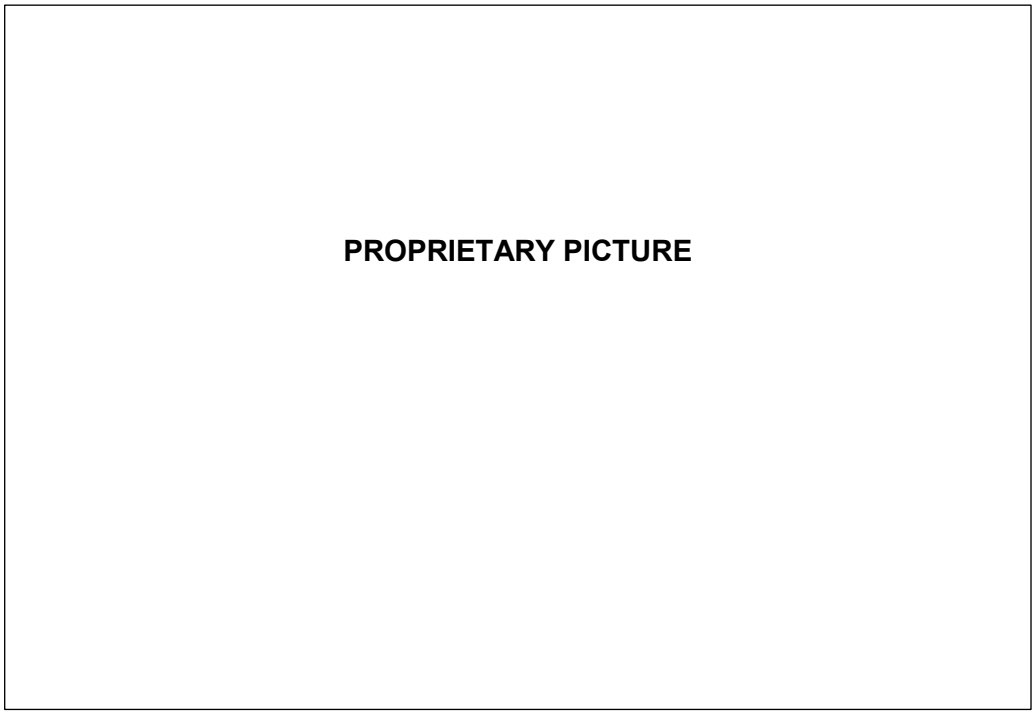

Figure 15
Representation of multiplicative coefficients

PROPRIETARY PICTURE

Figure 16
Bending of 900 MWe bottom span – Zircaloy-4 material

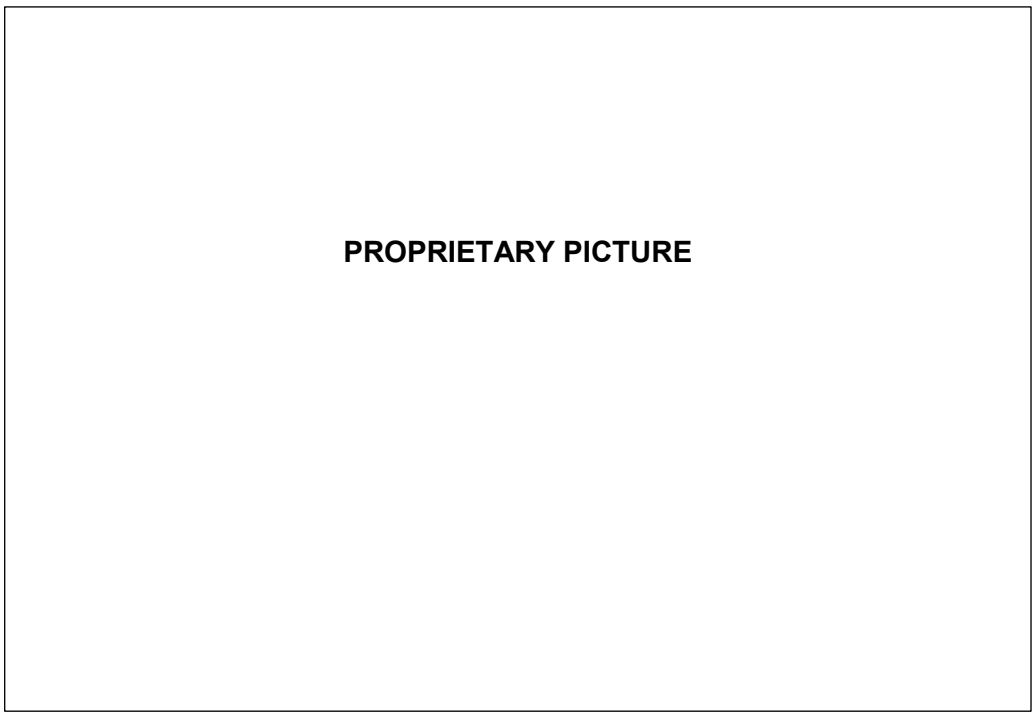

Figure 17
Bending of 900 MWe lower span – Force / deflection curves obtained

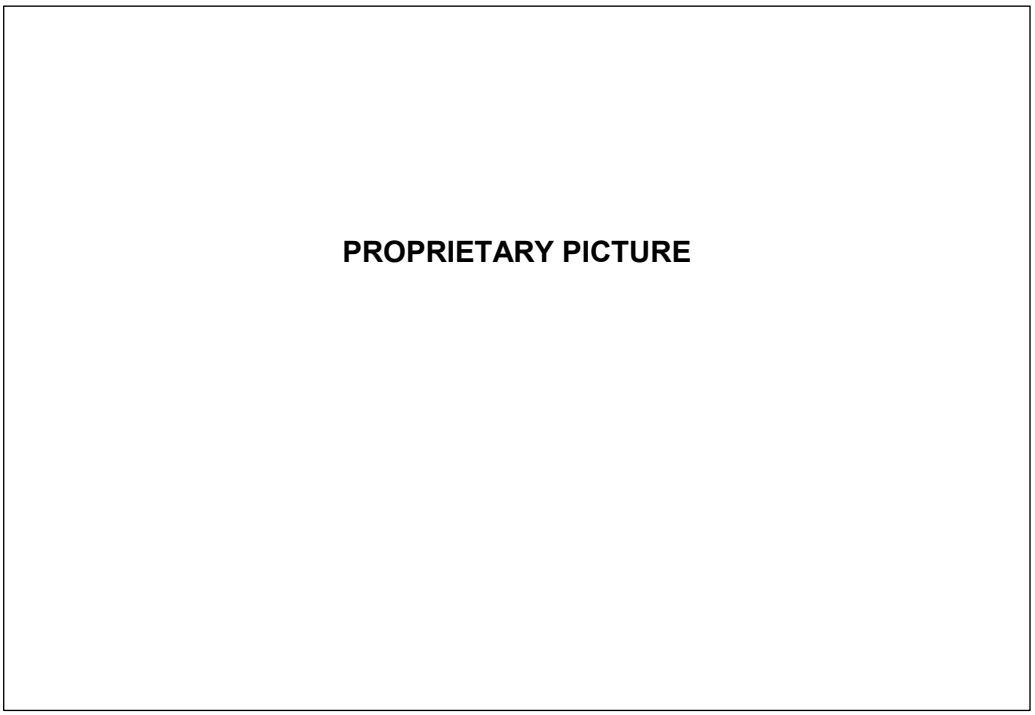

Figure 18
Bending of 900 MWe lower span – Force / deflection curves obtained for M5

[redacted]

spec min *= minimum specification at 20°C in quasi-static strain*
[redacted] *= extrapolated equivalent minimum specification in dynamical traction (see §4.2.3.4.2)*

PROPRIETARY PICTURE

Figure 19
Bending of 1300 MWe bottom span – Force / deflection curves obtained at 20°C and [redacted]

PROPRIETARY PICTURE

Figure 20
Bending of 1300 MWe lower span – Force / deflection curves obtained for M5
at -40°C and [redacted] °C for [redacted]

PROPRIETARY PICTURE

spec min *= minimum specification at 20°C in quasi-static strain*
[redacted]*= extrapolated equivalent minimum specification in dynamical traction (see §4.2.3.4.2)*

Appendix 1
Determination of the moment / curvature relationship

To carry out this calculation, the cladding section is split up into [redacted] plane sections of thickness [redacted] mm. For each section, the associated section (width * thickness) is determined as shown below.

PROPRIETARY PICTURE

PROPRIETARY PICTURE

The following calculation uses classical material strength hypotheses:

- The cross sections remain straight and non-deformable[1],
- The bending mid-axis is merged with the tube axis[2]

The input is the radius of curvature (reverse of the curvature). Based on this value, the following are determined for each basic section:

- Total elongation: ratio of the distance, from the relevant section to the mid-axis, over the radius of curvature,
- The stress corresponding to this elongation (interpolation in the material tensile curve),
- The tensile / compressive force in the section (product of the stress and the basic section),
- The corresponding basic moment (product of the force and the distance to the tube axis),
- The total moment (sum of the basic moments).

The calculation is carried out with each material, for radii of curvature between [redacted] mm and [redacted] m, with a progression optimized to have a best-fitted curve.
In the elastic zone, the moment / curvature ratio is constant and equal to the product [redacted] ([redacted]).
The curves obtained are shown on the figure below.

[1] The deformation of the cladding section is prevented by the presence of the pellets
[2] This hypothesis is obviously not realistic for a rod containing pellets. It is discussed in § 4.2.3.4.6

PROPRIETARY PICTURE

Appendix 2
Simulation calculation with CASAC

This software developed by AREVA-NP is used to address a number of problems by means of structural elements (beams, springs, masses, contact, sliding). It is particularly fitted to address geometrical non-linearities such as those of the bowed beam but is limited to the elastic domain.

The computer model takes into account the symmetry of the tested specimen and therefore addresses the case of a clamped / free beam of half length, i.e. [redacted] mm. The total length of the beam is however [redacted] mm to enable the displacement of the support point. The force application point strictly represents the reality of the test (support by a castor of diameter [redacted] mm). The inclination of the force with respect to vertical also changes versus beam rotation at the point of contact. The model schematic is illustrated below.

[redacted]

PROPRIETARY PICTURE

To extend the operating range of CASAC to plasticity, the previously determined moment / curvature relationship is introduced by means of an iterative procedure. For this purpose, the Young's modulus E in each section is replaced by an apparent module E' such that:

[redacted] plastic

[redacted] elastic

Hence: [redacted]

Note that the bending moment can be considered as [redacted] for each section, owing to the greatly reduced length of the latter.

To reduce computing time, the moment / curvature relationship is established once and for all for each material. Interpolating these results gives the curvature of each section versus the applied moment.

The rod / castor point of contact is defined by the coordinates:

[redacted]

Hypothesis: the rod / castor friction is null (the castors are made up of ball bearings)

The forces in the general coordinate frame are written:

[redacted]

The control of the iterations is carried out on the oblique force F .

The result is expressed in the form: [redacted] by analogy with the results of the bending tests. Note that for reasons of symmetry, force Fy is only half of the force measured in the test.

Note also that this methodology is only applicable when force F is [redacted]. Beyond this point, convergence is no longer possible as the calculation must be force-controlled to impose the angle of orientation of this force.

Appendix 3
Simulation calculation with an EXCEL spreadsheet

In parallel with the previous calculation and on a totally separate basis, a calculation is carried out with an EXCEL spreadsheet.

The EXCEL model represents [redacted] elements of [redacted] mm each, making a total beam length of [redacted] mm. The programming of the main equations (calculation of the moments, rotations, deflections, management of the contacts and convergence iterations) is done with a VBA module.

The calculation is carried out along the same lines as with CASAC. In particular, the moment / curvature relationship is identical. The application of the force (module, point of application and inclination) is managed in the same way as with CASAC. The coordinates of the nodes are updated after each calculation step to take into account the results of the previous step. These values are stored for each calculation step in 4 EXCEL spreadsheets (flèches_X, flèches_Y, Rotation and Moment). A fifth sheet is used to store the summing-up of the results.

The major difference from the CASAC calculation is that there is no iteration on a calculation step, except that of the force module, which provides control of the deflection increment. The error on the force / deflection relationship (linked to the geometrical non-linearity) is very small owing to the greatly reduced deflection increments (the latter are between [redacted] mm at start of compression and [redacted] mm towards the end). On the other hand, this method manages the positive or negative force module variations without risk of divergence.

The required precision regarding convergence iterations is [redacted] %.

This enables large deflections to be achieved for the rod, which could not be reached by CASAC.

Appendix 4
Simulation of the actual drop case

This calculation considers a 900 MWe rod section between its bottom end and the axis of grid 2. The calculation model is presented below.

PROPRIETARY PICTURE

The calculation is carried out with an EXCEL spreadsheet in the same way as for the previous calculation. For this calculation, the model used is changed as shown below:

PROPRIETARY PICTURE

The model features [redacted] elements. The section lengths are [redacted] mm close to the clamping and the support for proper control of the elongations and contacts and for the sake of consistency with the previous calculations, and [redacted] mm in the central part of the beam.

For each calculation step, the convergence iterations involve determining the force and moment values such that:

- The deflection at the support is less in absolute value than a criterion of [redacted] mm,
- The rotation at the support is equal to the ratio of the moment to the rotation stiffness with an accuracy better than [redacted] %.

The calculation is carried out for deflection increments between [redacted] and [redacted] mm: the total number of iterations is equal to [redacted]. For information, one calculation takes [redacted] to [redacted] min on a desktop computer.

The numerical inputs are as follows:

- L = [redacted] mm (fixed value during the calculation)
- b = [redacted] mm (variable value: the total length of the deformed beam is invariable)
- Kθ = [redacted] m.N/rd (value adopted for better consistency of the displacements at one quarter and three quarters of the span).

In parallel and for the purpose of verification, the calculation is also carried out by means of the CASAC software. The model features [redacted] elements of [redacted] mm each. The loading is applied as an apparent gravity to an object which is assigned a density. The calculation is carried out in large displacements for the following cases:

- Perfectly elastic material
- Zr-4 materials (use of the moment / curvature relationship previously established).

The plasticity is taken into account as in the previous calculation (see appendix 2). For this calculation using CASAC, the iterations involve determining the initial position of the pointwise contact such that after deformation, the support is located at a distance of [redacted] mm (±[redacted] mm).

The comparison of the results for a perfectly elastic material and for Zircaloy-4 is shown in figure A4.1. The near-perfect matching of the results helps to validate the calculation.

The moment / curvature relationships of the materials with the minimal properties designated by Zr4_min and M5_min are established in the same way as for the materials with nominal properties, by assigning to the bending moment a multiplier established on the basis of the bending test simulation (see figure 11).

Given the consistency of the calculations, only the results of the EXCEL calculations are used hereafter.

Regarding the calculation of the 1300 MWe configuration, the total number of elements ([redacted]) is kept. The length of the elements is considered to be similar between the 2 supports ([redacted] mm and [redacted] mm). The length of the elements beyond the support is reduced to [redacted] mm instead of [redacted] mm. The applied force values are obviously adjusted to obtain the desired deflections and deflection increments.

Otherwise, the calculations are strictly identical.

Figure A4.1

PROPRIETARY PICTURE